THE ASTRONOMICAL JOURNAL VOLUME 113, NUMBER 1 JANUARY 1997

AN OPTICAL STUDY OF THE CIRCUMSTELLAR ENVIRONMENT AROUND THE CRAB NEBULA

ROBERT A. FESEN

6127 Wilder Laboratory, Department of Physics and Astronomy, Dartmouth College, Hanover, New Hampshire 03755
Electronic mail: fesen@parsec.dartmouth.edu

J. MICHAEL SHULL[1]

Center for Astrophysics and Space Astronomy Campus Box 389, University of Colorado, Boulder, Colorado 80309
Electronic mail: mshull@casa.colorado.edu

ALAN P. HURFORD

Department of Physics and Astronomy, Dartmouth College, Hanover, New Hampshire 03755
Electronic mail: hurford@nebula.dartmouth.edu

Received 1996 May 26; revised 1996 October 8

ABSTRACT

Long-slit spectra of two peripheral regions around the Crab Nebula show no Hα emission down to a flux level of 1.5×10^{-7} erg cm^{-2} s^{-1} sr^{-1} (0.63 Rayleigh), corresponding to an emission measure limit of 4.2 cm^{-6} pc (3σ) assuming $A_V=1.6^m$ and $T_e=7000$ K. This is below the flux levels reported by Murdin & Clark [Nature, 294, 543 (1981)] for an Hα halo around the Crab. Narrow Hβ emission as described by Murdin [MNRAS, 269, 89 (1994)] is detected but appears to be Galactic emission unassociated with the remnant. A review of prior searches indicates no convincing observational evidence to support either a high- or low-velocity envelope around the remnant. Spectral scans confirm a well-organized, N-S expansion asymmetry of the filaments with a $\sim$500 km s^{-1} central velocity constriction as described by MacAlpine *et al.* [ApJ, 342, 364 (1989)] and Lawrence *et al.* [AJ, 109, 2635 (1995)] but questioned by Hester *et al.* [ApJ, 448, 240 (1995)]. The velocity pinching appears to coincide with an east-west chain of bright [O III] and helium-rich filaments. This expansion asymmetry might be the result of ejecta interaction with a disk of circumstellar matter, but such a model may be inconsistent with H and He filament abundances in the velocity constriction zone. A re-analysis of the remnant's total mass suggests that the filaments contain 4.6 ± 1.8 $\mathcal{M}_\odot$ in ionized and neutral gas, about twice that of earlier estimates. For a 10 $\mathcal{M}_\odot$ progenitor, this suggests that $\simeq$4 $\mathcal{M}_\odot$ remains to be detected in an extended halo or wind. © *1997 American Astronomical Society.* [S0004-6256(97)01901-8]

1. INTRODUCTION

The presence of hydrogen in its filaments technically classifies the Crab Nebula as a Type II supernova remnant (SNR). However, because of its low-mass, helium-rich ejecta (up to $Y=0.90$–0.95 by mass) and slow expansion, it has long been recognized as an atypical SNR. For example, the Crab has an anomalously small kinetic energy. The brighter filaments expand at $\leq$2000 km s^{-1} (Clark *et al.* 1983; Fesen & Ketelsen 1985; Lawrence *et al.* 1995), considerably less than the 5000–10 000 km s^{-1} typically observed in Type II SNe. When combined with an estimated nebula mass of 1–2 $\mathcal{M}_\odot$ (MacAlpine & Uomoto 1991), this relatively slow expansion implies a kinetic energy of $10^{49.5}$ ergs, some 30 times lower than the canonical 10^{51} ergs for Type II SNe. This energy is really only an upper limit since much of the nebula's expansion derives from the pulsar wind. Despite this, the Crab SN (1054 AD) was apparently not subluminous optically, with historic sightings suggesting a peak visual brightness of -4 to -6 mag (Clark & Stephenson 1977; Pskovskii 1978). This translates into $M_V=-18\pm1$ mag assuming a distance of 2 kpc (Trimble 1973) and an optical extinction $A_V=1.6^m$ (Miller 1973).

Supernova models suggest that the Crab's progenitor mass was 8–13 $\mathcal{M}_\odot$ (Nomoto *et al.* 1982; Nomoto 1985, 1987) corresponding to spectral types B4 V–B1.5 V (Vacca *et al.* 1996). This mass range is constrained by the presence of the Crab pulsar, which establishes a lower limit of 8 ± 1 $\mathcal{M}_\odot$, and the low oxygen and carbon abundances in the filaments, which place an upper limit of 13 $\mathcal{M}_\odot$ based on nucleosynthesis models. With an ionized nebula mass of 1–2 $\mathcal{M}_\odot$ and 1.4 $\mathcal{M}_\odot$ in the pulsar, some 4–10 $\mathcal{M}_\odot$ remains undetected in and around the Crab or in post main-sequence mass loss.

Several solutions have been put forth to explain the Crab Nebula's small kinetic energy and mass. Nomoto (1985, 1987) proposed that the Crab was formed by an underenergetic explosion of a red-giant helium star (see also Wheeler 1978). Post-main-sequence progenitor mass loss might lead

[1]Also at JILA, University of Colorado and National Institute of Standards and Technology.

 0004-6256/97/113(1)/354/10/$10.00

to high He/H ejecta with filament abundance variations due to interactions with surrounding H-rich circumstellar matter. However, models that match the estimated filament CNO abundances require a delicate tuning of CNO destruction and dredge-up and are only marginally consistent with the observations. Alternatively, Chevalier (1977, 1985) and Chevalier & Fransson (1992) suggested that an appreciable amount of the Crab's missing mass and energy lies in a fast, H-rich halo surrounding the familiar bright nebula. A H-rich envelope moving at 5000 km s^{-1} could resolve the Crab's low kinetic energy problem and bring the Crab SN more in line with the high-velocity hydrogen emission commonly seen in Type II SNe. An extended progenitor envelope could also produce a brighter SN, possibly reconciling the reported brightness of the 1054 AD event with the remnant's low kinetic energy. It could even help in understanding continuing filament development in the remnant (Hester *et al.* 1996). However, such a halo would be limited, on kinetic energy considerations, to a mass of

$$\mathscr{M}_{\rm halo} < (4.\mathscr{M}_{\odot}) \left(\frac{E_{\rm SN}}{10^{51}\ {\rm erg}} \right) \left(\frac{V_{\rm halo}}{5000\ {\rm km\ s^{-1}}} \right)^{-2}. \quad (1)$$

Chevalier's high-mass, high-velocity envelope could be detected either by extended optical emission, nonthermal radio emission from a fast shock advancing through the ambient interstellar medium, or through a steeper spectral index at the shock front along the Nebula's outer edge. Although emission from a fast shock would be faint given the low interstellar density around the Crab (Romani *et al.* 1990; Wallace *et al.* 1994) at its location 200 pc below the Galactic plane, several searches have been made for a fast shell or extended halo. Observations in the radio (Wilson & Weiler 1982; Velusamy 1984, 1985; Trushkin 1986; Velusamy *et al.* 1992; Frail *et al.* 1995), x-rays (Mauche & Gorenstein 1989; Predehl & Schmidt 1995), and optical (Gull & Fesen 1982; Fesen & Ketelsen 1985) have failed to detect any extended or outer shell emission. The only claimed detections have been in the optical by Murdin & Clark (1981) who found a $6' \times 14'$ radius halo on a deep Hα Schmidt glass plate and by Murdin (1994) who reported faint, narrow Hβ emission outside the northern edge of the remnant. These results suggest an Hα halo surface brightness of $\sim 2 \times 10^{-7}$ erg cm^{-2} s^{-1} sr^{-1}.

In this paper, we report the results of an optical search for both an extended optical halo through hydrogen line emission and pre-SN, circumstellar material through asymmetries in the Crab's filamentary expansion. We also critically reexamine the remnant's filament mass estimates.

2. OBSERVATIONS

2.1 Halo Spectra

Following Murdin (1994), we obtained low dispersion spectra along the Crab's northwestern edge and northern jet [see Fig. 1 (Plate 15)]. The data were taken in 1994 December under photometric conditions using the Michigan-Dartmouth-MIT (MDM) 2.4 m Hiltner telescope and the Mark III spectrograph with a 600 line mm^{-1} grism (4600 Å blaze), a $2.36'' \times 4.6'$ E-W slit, and a 1024×1024 Tektronix CCD detector. The wavelength region covered was 4300–6800 Å with a spectral resolution of 2.5 Å $pixel^{-1}$. Along the remnant's NW edge, the slit was positioned across Star #4 (Wyckoff & Murray 1977) and extended about 3.4′ west of the sharp [O III] western limb (see Gull & Fesen 1982). Three 3000 s exposures were taken, interleaved with equal-length sky exposures at a location 16.6′ north and 7.5′ west, towards the Galactic plane.

Spectra across the Crab's northern emission jet were obtained with an E-W slit positioned through a bright star near the jet's center. These data provide an easy comparison of emission-line strengths from a possible halo with the jet's faint Hα emission. Three 2500 s exposures were obtained, interleaved with equal sky exposures taken 12.0′ west and 13.4′ north, at nearly the same blank sky region observed for the NW limb data. For both NW and jet spectra, object and sky exposures were separately co-added and reduced using standard IRAF software, Xe-Hg-Ne comparison lamps, and Oke (1974) and Stone (1977) spectral standards.

2.2 Scan Spectra

To examine global filament expansion patterns, we also obtained two-dimensional spectral scan images like those of MacAlpine *et al.* (1989). The Crab Nebula was scanned in both N-S and E-W directions across various portions to produce integrated velocity maps. In 1992 November we obtained a long-slit scan spectrum using the same telescope and instrument setup as for the halo observations. The $1.7'' \times 4.6'$ slit gave a spatial resolution of $0.73''$ $pixel^{-1}$ and spanned nearly the remnant's entire N-S extent. The slit was scanned E-W across just the inner 2′ portion of the Crab, approximately between the remnant's east and west synchrotron "bays" (Fesen *et al.* 1992). Three 1200 s exposures, each consisting of ~16–20 E-W scans, were co-added, bias subtracted, and flat-field corrected.

Long-slit scans were also obtained in 1993 September using the MDM 1.3 m McGraw–Hill telescope and the Mark III spectrograph. A 1024×1024 Tektronix CCD and 600 lines mm^{-1} transmission grisms yielded 2.5 Å $pixel^{-1}$ dispersion, $1.6''$ $pixel^{-1}$ spatial resolution, and wavelength coverage from 4500 to 7000 Å. Three 900 s E-W scans of the entire remnant were taken, using a $1.5'' \times 8'$ N-S aligned slit. The starting and ending points were 10^s west and 12^s east of the pulsar. Three 1000 s exposures were also taken, scanning in the E-W direction over just the central 1′ wide region, centered on the remnant's expansion point as defined by Wyckoff & Murray (1977). The slit was then rotated 90°, and the entire nebula scanned in the N-S direction. Finally, three 1000 and 600 s exposures were taken, covering the remnant's inner 1′ and 4′ sections respectively. Each set of scans was individually co-added, bias subtracted, and flat-field corrected. Sky subtraction was accomplished using outer portions of the slit beyond the remnant's edge. As an aid in detecting weak features, continuum objects such as field stars and the Crab's synchrotron emission were removed by fitting the observed continuum at each point along the slit using averages in spectral regions free of strong emission lines.

3. Hα EMISSION AROUND THE CRAB NEBULA

3.1 Background

Using a IIIaF plate and a 150 Å wide Hα filter on the 1.2 m UK Schmidt telescope, Murdin & Clark (1981) detected a faint, diffuse halo beyond the nebula's nominal boundary. The emission extended 6′ outward along the minor axis and 14′ along the major axis as measured from the remnant center (see Murdin 1994 for greyscale reproductions of the Schmidt image). The halo's average Hα surface brightness was $\sim 2\times10^{-7}$ erg cm^{-2} s^{-1} sr^{-1} (0.83 Rayleigh) corresponding to an emission measure EM≃7.7 cm^{-6} pc, for $T=10^4$ K and $E(B-V)=0.52$, based on a measured $A_V=1.6^m$ (Miller 1973). The emission decreased with radial distance, and the surface brightness near the nebula's edge was several times larger than the quoted average value. Although the match of the halo's elliptical shape and orientation with that of the main nebula might indicate an instrumental origin (Davidson & Fesen 1985; Chevalier 1985), Murdin and Clark argued that an analysis of the image's point-spread function showed that the halo was not scattered light.

Murdin (1994) expressed doubts that the detected halo contains high-velocity material due to a lack of spectroscopic and imaging evidence indicating the presence of high-speed knots. However, through an examination of La Palma archival blue spectra taken across the Crab's northwest edge and the northern jet with the 2.5 m Isaac Newton telescope, Murdin found narrow (FWHM≤60 km s^{-1}), low-velocity (~0 km s^{-1}) Hβ emission around the remnant. This emission seemed to abruptly fade at the remnant's limb and no similar emission was seen in [O III] λ4959,5007, unlike the Nebula's outer filaments which exhibit high [O III]/Hβ (Gull & Fesen 1982). Based on these properties and an apparent r^{-3} emission falloff, Murdin argued that the emission was unlikely to be diffuse Galactic emission, Instead, he suggested an origin in a low-velocity, stellar wind from the Crab progenitor during its red giant phase. From the measured Hβ line flux, he estimated a total halo mass of ~4 $\mathcal{M}_\odot$.

3.2 Long-Slit Spectral Results

Our long-slit spectra obtained at the northwestern edge and northern jet show no hydrogen line emission outside of the Crab's sharp optical boundaries. A two-dimensional display of the sky-subtracted NW edge spectrum (Fig. 2) covers Hα, [N II] λλ 6548,6583, [S II] λλ 6716,6731, and [O I] λλ 6300,6364 emission along the 275″ long slit extending east to west (left to right) across the Crab's western limb (see Fig. 1). The continuum source near the edge of the strong line emission is the Wyckoff & Murray (1977) Star #4, situated about 24″ east of the Crab's western edge as seen in the [O III] images of Gull & Fesen (1982). A plot of sky-subtracted counts versus E-W distance along the slit for the Hα wavelength region (6563±5 Å) is also shown. Neither narrow nor broad line emission is seen for Hα, [N II], [S II], or [O III] λ5007 west of the remnant's sharp [O III] edge out to a distance of ~3.4′.

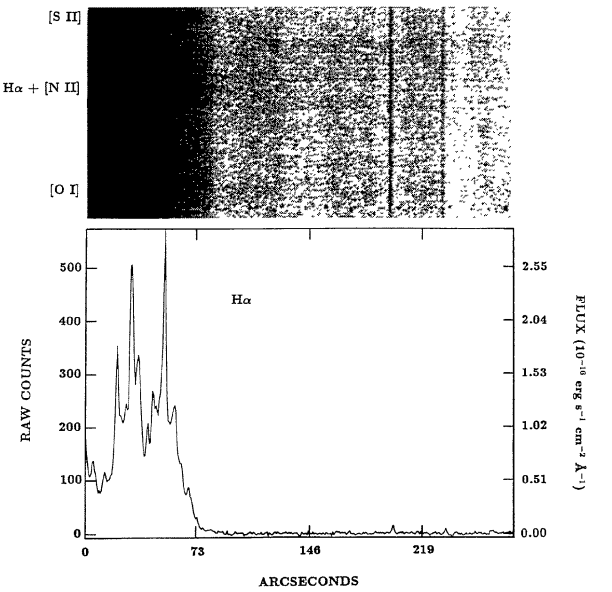

FIG. 2. Negative greyscale display of E-W long-slit spectrum taken across Crab's NW limb (left to right) covering the wavelength region 6275–6750 Å (bottom to top) along with a plot of raw counts and corresponding flux for Hα along the slit. White vertical sections along the slit are due to sky oversubtraction by faint stars present in the sky spectrum slit.

We can set an upper limit for Hα emission using 41-pixel sections along the 2.36″ slit, equivalent to 70.64 arcsec^2 (1.66×10^{-9} sr). In all sections examined, we measured an rms of 1.2×10^{-17} erg cm^{-2} s^{-1} Å^{-1} across the 6300–6700 Å region, corresponding to a 3σ line strength limit (FWHM=7 Å) of 2.5×10^{-16} erg cm^{-2} s^{-1}. This translates into a surface brightness of 1.5×10^{-7} erg cm^{-2} s^{-1} sr^{-1} or 0.63 Rayleigh. A similar emission limit is found in velocity space corresponding to a linewidth of 4700 km s^{-1}. While our surface brightness upper limit is only a little below Murdin & Clark's reported 2×10^{-7} erg cm^{-2} s^{-1} sr^{-1} average halo value, it is three to four times less than they reportedly detected along the nebula's limbs (see Fig. 5 of Murdin 1994).

Emission measure (EM) in units cm^{-6} pc is given by

$$\mathrm{EM}=2.77\left(\frac{T}{10^4\ \mathrm{K}}\right)^{0.936} I(\mathrm{H}\alpha)\exp[2.33E(B-V)], \qquad (2)$$

where T is the electron temperature, $E(B-V)$ is the measured color excess to the Crab Nebula, and $I(\mathrm{H}\alpha)$ is the line intensity (in Rayleighs). Equation (2) is an updated version of a similar formula (Reynolds 1988) used by Murdin (1994), but with newer recombination rates (Osterbrock 1989) and the selective extinction curve of Cardelli *et al.* (1989), for which $A_{\mathrm{H}\alpha}=0.818A_V$, $A_V=3.1E(B-V)$, and $\tau(\mathrm{H}\alpha)=2.33E(B-V)$. Adopting an electron temperature of 7000 K (Murdin 1994), we estimate a limit of EM≤4.2 cm^{-6} pc.

An EM upper limit of ≃4 cm^{-6} pc can also be set from our spectrum across the northern jet. Figure 3 shows a two-dimensional display of the spectrum obtained there, containing Hβ, [O III] λλ 4959,5007, Hα, [N II] λ6583, and [S II] λλ 6716,6731 emission from the ~47″ wide jet. This figure also

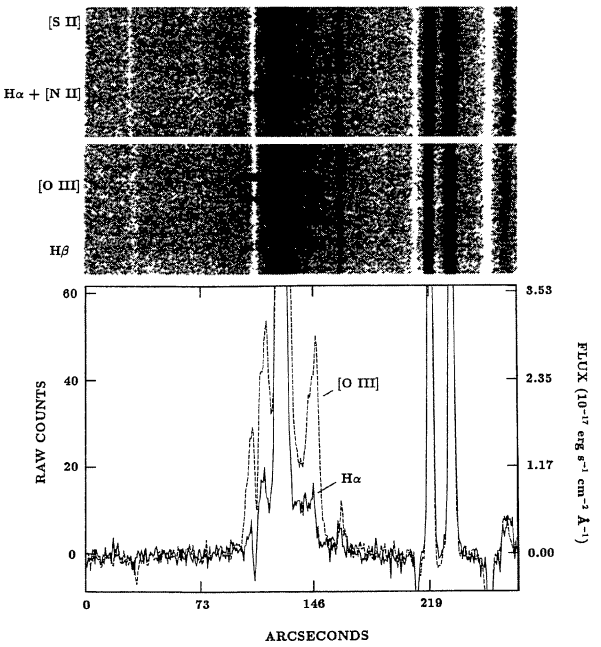

FIG. 3. Negative greyscale displays of long-slit data taken across Crab's northern emission jet covering the wavelength regions of Hα, [N II], [S II], and [O III] and Hβ. The raw counts for Hα (solid line) and [O III] λ5007 (dashed line) along the slit are also plotted, summing over 9 pixels (=22.5 Å). The corresponding flux for Hα is shown on the right-hand-side vertical axis. White vertical sections along the slit are due to sky over-subtraction of faint stars present in the sky spectrum slit.

shows east-west cuts at [O III] λ5007 and Hα, where we summed over nine pixels (22.5 Å, 1025–1350 km s^{-1}) to search for high-velocity Hα and [O III] halo emission. These plots indicate that at this location, some 50″ above the Crab's northern limb, any halo emission must be weaker than ~25% in Hα and ~10% in [O III] λ5007 relative to the jet's east-west limb walls.

Hester *et al.* (1996) argue that a high-velocity halo containing as much mass as in the bright nebula might elude easy spectroscopic detection due to large linewidths. Consequently, the actual Hα emission measures of a surrounding halo might be well below those reported by Murdin & Clark (1981). However, decreasing line widths towards the halo's edge, where added limb emission due to the fast halo's shock interface with the ambient interstellar medium, might make a faint, fast halo more detectable. Moreover, some degree of clumping of the high-velocity material is likely, increasing the emission measure.

Let us now estimate what one would expect to observe. We assume that, prior to the Crab explosion, a steady red-giant wind was blowing for $(10^6\ \mathrm{yr})t_6$ at a velocity $(10\ \mathrm{km\ s^{-1}})V_{10}$. The red-giant wind would then have a maximum extent of

$$R_{\max} \approx (10\ \mathrm{pc}) V_{10} t_6, \tag{3}$$

so that $R_{\max} \gg R$, where $R=(1.75\ \mathrm{pc})d_2$ is the mean shell radius for an assumed Crab distance of $(2\ \mathrm{kpc})d_2$. If the mass-loss rate was $\dot{\mathscr{M}}=(10^{-5}\mathscr{M}_\odot\ \mathrm{yr}^{-1})\dot{\mathscr{M}}_{-5}$ and He/H =0.1 by number, the wind at radius r would have a hydrogen density,

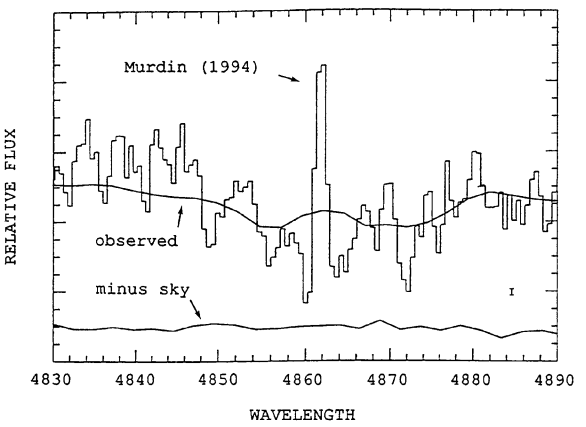

FIG. 4. Murdin's (1994) high-dispersion spectrum of the sky near the Crab (ragged line), with our lower-dispersion data (smooth lines) for both raw (observed) counts and after subtraction of neighboring emission. Our spectra are plotted with arbitrary flux offsets to Murdin's data. The error bar (1σ) at bottom right refers to our data. Note the disappearance of the weak Hβ emission after sky subtraction.

$$n_{\mathrm{H}}(r) = (0.74\ \mathrm{cm^{-3}})\dot{\mathscr{M}}_{-5} V_{10}^{-1} \left(\frac{R}{r}\right)^2. \tag{4}$$

This gas will be kept fully photoionized by the Lyman continuum photons, $N_L \approx 10^{46}$ photons s^{-1}, produced by the pulsar (Davidson & Fesen 1985). For singly ionized H and He, the emission measure through the r^{-2} wind, just outside the Crab limb, would be

$$\mathrm{EM} = \frac{\pi R}{2}[n_e(R)]^2 = (1.8\ \mathrm{cm^{-6}\ pc})\dot{\mathscr{M}}_{-5}^2 V_{10}^{-2} d_2. \tag{5}$$

Our observed limits are about three times above this value (EM<4.2 cm^{-6} pc), which constrains the ratio $\dot{\mathscr{M}}/V_{10}$. Out to radius $R_{\max}$, the steady wind would contain a mass

$$\mathscr{M}(r<R_{\max}) = (1.7\mathscr{M}_\odot)\dot{\mathscr{M}}_{-5} V_{10}^{-1} d_2 \left(\frac{R_{\max}}{R} - 1\right), \tag{6}$$

which, for $(R_{\max}/R) \approx 5-6$, is also comparable to the expected $\sim 4\mathscr{M}_\odot$ in the wind.

While emission measure limits might need to be pushed about a factor of 3–10 lower to detect such a wind, a low-density halo ($n_{\mathrm{H}} \leq 1$ cm^{-3}) could be indirectly detected by an increase or change in ionization of the nebula at the interface with the inner halo boundary. Our NW spectrum extended more than 3′ off the Crab's western edge, yet no anomalous [O III] emission was seen either distant or near the remnant's western limb (Fig. 2). The same was true across the jet along the remnant's northern edge (Fig. 3). Therefore, although we could detect no extended Hα emission at the level reported by Murdin & Clark or any evidence of material outside the visible remnant boundary, a substantial mass of surrounding material with lower emission measures is still possible.

Finally, we investigated the faint Hβ emission surrounding the Crab reported by Murdin (1994). While we also found faint, narrow Hβ (and Hα) emission around the Crab, contrary to Murdin's conclusion, this emission appears to be diffuse galactic emission (Reynolds 1988) unassociated with

the remnant. In Fig. 4, we reproduce Murdin's spectrum of the sky near the Crab along with our lower-dispersion spectrum taken along the remnant's NW edge. We detected, but at a much lower resolution, the faint Hβ emission that Murdin reported. But we found that similar strength Hβ emission in a blank sky region located $\sim$15′ to the northwest, well outside the suspected halo. Consequently, the Balmer line emission seen near the Crab Nebula virtually disappears after subtraction of the sky spectrum (see Fig. 4). We also found, as Murdin did, that the Hβ emission seemed to fade near the Crab's optical edge. However, this appears to be the result of lower signal-to-noise as this weak emission signal becomes lost in the synchrotron emission at the remnant's boundary.

3.3 Other Halo Search Data

Deep Hα images of the Crab in the literature often detect its faint northern jet, but do not show any surrounding diffuse emission (e.g., Gull & Fesen 1982; Marcelin *et al.* 1990). It is therefore surprising that Murdin & Clark's halo discovery plate does not detect the presumably brighter northern jet feature (see Figs. 1 and 2 in Murdin 1994). Several uncalibrated Hα images of the Crab taken by us using a variety of instruments easily detect the remnant's northern jet but not a halo. These include a 2000 s Hα exposure on the 0.6 m KPNO Schmidt (FOV=68′, 2.0″ pixel^{-1}, filter=20 Å FWHM) and a series of 300 s exposures on the 1.3 m MDM telescope (FOV=15′, 1.76″ pixel^{-1}, filter=80 Å FWHM). Our KPNO Schmidt image also shows no knots or filaments out to a radius of 25′ at a comparable brightness level to that seen in the jet.

It is difficult to understand how CCD images could miss narrow, Balmer line emission, as described by Murdin (1994) but be detected on a Schmidt photographic plate using a 150 Å filter. Likewise, if a high-velocity halo was missed in CCD imaging owing to the use of filters narrower than the 150 Å one employed by Murdin & Clark (1981), then deep, sky-subtracted CCD spectra of the jet taken with larger aperture telescopes should have seen it (Shull *et al.* 1984; Marcelin *et al.* 1990; Fesen & Staker 1993; this paper). Alternatively, if the halo is of low density and high ionization, as described by Lundqvist *et al.* (1986), then one might expect it to be at least as bright in [O III] emission as in Hα. However, no [O III] images of the remnant show any diffuse or filamentary emission beyond the nebula's sharp boundaries (Gull & Fesen 1982; Véron-Cetty *et al.* 1985; Fesen & Gull 1986; Marcelin *et al.* 1990; Fesen & Staker 1993), and spectra limit high-velocity [O III] emission down to a level of 2×10^{-17} erg cm^{-2} s^{-1} arcsec^{-2} (Davidson 1987).

Neither x-ray nor radio studies of the Crab support the existence of a halo or high-velocity shock around the remnant. Mauche & Gorenstein (1989) and Predehl & Schmidt (1995) find no excess x-ray emission around the Crab above that expected from interstellar dust scattering of the remnant's x-ray emission. Frail *et al.* (1995) place strong 333 MHz radio emission limits to any high-velocity material associated with the Crab Nebula down to a limit of $\leq4.3\times10^{-22}$ W m^{-2} sr^{-1} Hz^{-1}. This restricts any shock radio emission around the Crab to two orders of magnitude below that of the SN 1006 remnant, an unusually weak radio SNR. Thus, within a radius of 32′, any shell around the Crab must have a surface brightness far below that of any known Galactic SNR or possess a significantly reduced shock wave efficiency for accelerating relativistic particles. Frail *et al.* also found no spectral index steepening along the nebula's limb which might indicate a strong shock at the interface with the ambient interstellar medium. Finally, Bietenholtz *et al.* (1991) estimated a substantially lower interstellar density than possible for the suspected halo described by Murdin (1994).

In summary, our optical results, together with radio and x-ray data, fail to indicate the presence of a fast, massive envelope around the Crab Nebula as proposed by Chevalier (1977, 1985) on theoretical grounds. We note that the similarity in shape of the reported Murdin & Clark halo with that of the main nebula is also quite unexpected since the structure of any high-velocity halo would presumably have been determined by the dynamics of the ejected H-rich envelope, while the nebula's morphology has been affected by the pulsar's collimated, NW-SE wind.

4. INTERACTION WITH CIRCUMSTELLAR MATTER?

An alternative to the massive halo explanation for the Crab's low mass and kinetic energy is Nomoto's (1985, 1987) helium star explosion. As part of this model, the progenitor underwent substantial pre-SN mass loss, raising the potential for SN ejecta interaction with surrounding circumstellar matter. An ejecta-circumstellar interaction might help to explain abundance variations seen among the filaments (cf. Blair *et al.* 1992). Using low-dispersion, long-slit drift scans of the remnant, MacAlpine *et al.* (1989) found evidence for a central velocity constriction, implying a N-S bipolar expansion possibly associated with a torus of high-helium filaments. This N-S expansion asymmetry was also seen in the [O III] Fabry–Perot imaging data of Lawrence *et al.* (1995).

However, analysis of *HST* imaging does not indicate a N-S expansion (Hester *et al.* 1995). What is seen is a strong NW-SE cylindrical symmetry aligned with the remnant's main optical axis caused by the pulsar's strong relativistic wind. This NW-SE expansion axis is dramatically visible in Fabry–Perot imaging data as large holes in the distribution of the brightest filaments at either end of the major axis (Lawrence *et al.* 1995). This, together with the presence of a NW-SE symmetry axis on a broad range of spatial scales, led Hester *et al.* (1995) to doubt the significance of a N-S expansion axis. They instead suggested that a chance line-of-sight alignment of a central ring of filaments could explain the apparent expansion constriction.

These conflicting results leave unclear whether a N-S expansion asymmetry is important for understanding the Crab's expansion properties. Below, we examine this question using long-slit scans of the Crab Nebula, which provide a means of studying global filament expansion patterns in a number of bright emission lines. Such spectral scans integrate the remnant's velocity structure by relative line intensity, revealing expansion symmetries when the slit parallels an important

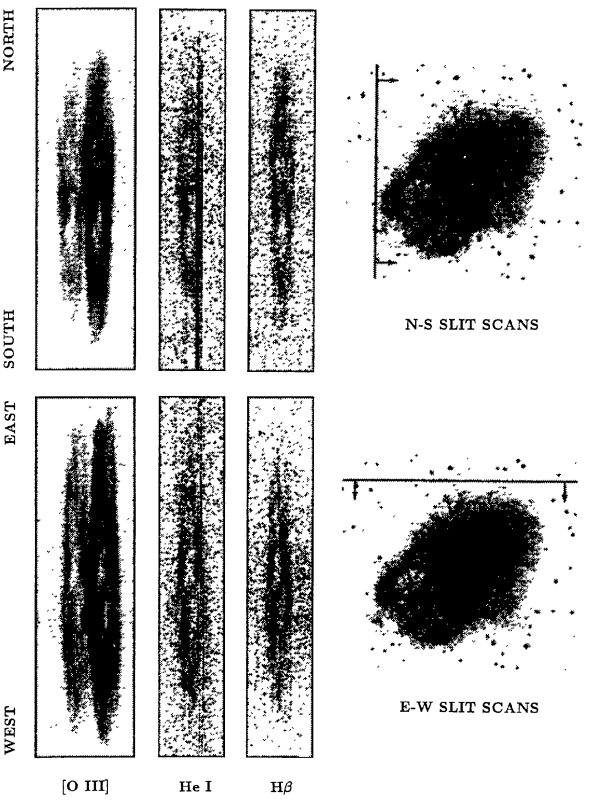

FIG. 5. Velocity structure present in the N-S slit (top) and E-W slit (bottom) scans across the remnant in the lines of [O III] λλ 4959,5007, He I λ5876, and Hβ λ4861.

axis for the brighter filaments. Our scans are of both higher spectral and spatial resolution than those of MacAlpine *et al.* (1989), and we investigate the Crab's velocity structure and relative intensities in lines other than just the [O III] λ5007 studied by Lawrence *et al.* (1995).

4.1 Long-Slit Scan Results

The top of Fig. 5 shows the velocity structure observed in the N-S slit scans across the E-W width of the remnant for the lines of [O III] λλ 4959,5007, He I λ5876, and Hβ. The data show a bipolar symmetry with the brighter filament emission concentrated in a central, pinched velocity structure ~30″ in N-S extent, most apparent in the bright [O III] lines. Faint emission within the apparent northern and southern expansion lobes arises partly from superimposed emission from low-velocity filaments situated along the remnant's east and west limbs.

Within the pinched expansion zone, the brighter [O III] filaments lie preferentially along the inner edge in agreement with the results of Lawrence *et al.* (1995). Since the filaments are photoionized by the pulsar's synchrotron nebula and are optically thin, a strong dependence of filament intensity with viewing angle is not expected. Consequently, these central, slow moving features are, in fact, the remnant's more luminous [O III] filaments.

Relative strengths of the He I and Hβ line emission in these scans are in line with the He/H emission variations within the filaments reported by Uomoto & MacAlpine (1987). While Hβ shows no strong preference for the central pinched zone (Fig. 5), He I is concentrated in this area. Despite the low signal to noise, the detection of few He I knots away from the central region (especially to the north) suggests a large He I/Hβ ratio among these central filaments. We find a mean ratio I(He I)/I(Hβ)≈0.8 in the pinch zone and ≤0.4 elsewhere. Since I(He I)/I(Hβ) closely follows N(He)/N(H) in the filaments (Henry & MacAlpine 1982), the most He-rich filaments are those lying within the constricted region. This indicates a link between the high helium band and the decreased filament velocities along this line of sight.

The bottom of Fig. 5 also shows the filament velocity structure using an E-W slit scanned N-S across the remnant. The region scanned was restricted to only the inner 4′ region to help suppress low-velocity, limb emission. Despite less confusion from the limb, the data show a poorly organized velocity pattern in these same lines. No expansion constriction in the filament is seen like that in the N-S slit scan data (above). In addition, the brighter filaments are distributed more randomly, with neither [O III] nor He I exhibiting the positional coherence visible in the N-S scan data.

The N-S bipolar expansion is better resolved in Fig. 6, (Plate 16) where the [O III] and Hβ velocity features are shown from N-S slit scans over the Crab's inner 2′ region. These data have nearly twice the spectral resolution (300 km s^{-1}) and spatial resolution of Fig. 5. The scans covered just the area between east and west bays, giving less contamination from low-velocity filaments from the east and west limbs that might mask velocity patterns. These data reveal a well-organized, hourglass-shaped filament expansion structure with a centrally pinched zone ~25″ in N-S length, narrowing to ±550 km s^{-1}. This low-velocity middle section is in contrast to that of the northern and southern regions, which expand at ±1150 and ±900 km s^{-1}, respectively.

The pinched expansion zone appears continuous and fairly symmetric in terms of rear and front hemisphere filament distributions. The declination of maximum velocity pinching lies near to, but ~5″ north of, the remnant's expansion center, as seen by the spectrum of Star #9 (Wyckoff & Murray 1977) whose declination lies within a few arcseconds of the remnant's estimated expansion point. North and south velocity bubbles appear well defined along their lower-velocity inner edges. The northern lobe is noticeably less symmetric, with some bright, less-redshifted emission and a break along the northern boundary leading to the remnant's northern jet. Other scans show that the shape of the N-S bipolar symmetry does not change appreciably over smaller inner sections and remains a strong feature in lines covering a wide ionization range, including [O I] λ6300, [S II] λλ 6716,6731, and He II λ4686.

4.2 The Meaning of a N-S Expansion Asymmetry

The difference between N-S and E-W scan data (Fig. 5) confirms the N-S expansion symmetry described by MacAlpine *et al.* (1989), but it does not yet prove that this is an important kinematic structure of the remnant. The ob-

served Δv for the pinched regions is $\sim$500 km s^{-1}. If there were other coherent filament rings with the same velocity dispersion within 45° of the plane of the sky, one would expect to see $\pm$350 km s^{-1} deviations from a smooth bipolar expansion. That fact that this is not seen (Fig. 6) shows that the N-S bipolar expansion is special to the remnant. This conclusion is supported by the concentration of the brightest and most chemically distinct (helium-rich) filaments in the pinched expansion zone.

How does this N-S expansion fit in with the Crab's obvious NW-SE cylindrical symmetry axis? This axis is associated with the pulsar's rotation axis and thus tied to the remnant's evolutionary development (Hester *et al.* 1995, 1996). It therefore is a post-SN feature, imprinted on the nebula's kinematics by the strong relativistic wind along the pulsar's rotation axis. The presence of faint synchrotron radio and optical emission leaking beyond the remnant's filamentary boundary along the remnant's NW limb (Velusamy 1984; Fesen *et al.* 1992) is additional evidence of this NW-SE wind and the low density of the ambient interstellar medium.

However, a N-S axis may be an equally important structure of the remnant since it dominates scan data taken over a range of spatial scales. The remnant's peculiar northern jet aligns with this axis (Fesen *et al.* 1992) as does polarization from the toroidal magnetic field associated with the synchrotron nebula (Michel *et al.* 1991). Fesen *et al.* (1992) also noted that the N-S jet axis is orthogonal to the plane formed by two prominent indentations (''E and W bays'') in the synchrotron nebula and a torus of helium-rich filaments in the inner nebula. Proper-motion measurements show the bays moving along a line that passes close to the remnant's expansion center and orthogonal to the N-S axis of the northern jet. Although Hester *et al.* (1995) suggest that the E and W bays could be random indentations produced by magnetic Rayleigh–Taylor instabilities in the nebula, an examination of Figs. 1 and 8 in Fesen *et al.* (1992) shows that the bays are, by far, the most prominent of such features. The orthogonality of the E-W bay axis to the bipolar outflow and northern jet, and the fact that the bays' E-W axis passes through the center of expansion, suggest that a N-S axis is an important feature of the nebula.

A N-S bipolar expansion could represent either an asymmetry in the SN explosion itself or a bipolar outflow caused by confinement of the expanding ejecta. Bipolar outflows in SNe have not been modeled in detail, and it may be difficult to match simultaneously the width and inner flatness of the pinched expansion zone. While expansion asymmetries have been seen in some SNe (e.g., SN 1987A and SN 1993J; Podsiadlowski *et al.* 1993; Marcalde *et al.* 1995), none show clear bipolar symmetry.

Stellar bipolar flows are common, although poorly understood features of a class of planetary nebulae (Bond & Livio 1990), high mass-loss stars like Eta Carina (Humphreys & Davidson 1994), and pre-main-sequence stars. Generally, bipolar outflows are thought to be caused by a thin surrounding disk of circumstellar material, possibly produced by the interaction of stellar winds. In SN 1987A, for example, an equatorial concentration of low-velocity circumstellar matter must have been present around the SN 1987A progenitor in order to produce the observed inner ring-like structure (Luo & McCray 1991; Blondin & Lundqvist 1993). Bjorkman & Cassinelli (1993) found that an equatorial disk can form around rapidly rotating Be stars due to ram-pressure confinement by the stellar wind. This mechanism requires rotational velocities in the range 230–300 km s^{-1} and is most common at spectral type B2, comparable to that of a 10 $\mathcal{M}_\odot$ Crab progenitor. In SN 1987 A, subsequent interaction of a fast (blue-supergiant) wind with a slow (red supergiant) wind produced surprisingly thin ring structures (Blondin & Lundqvist 1993; Martin & Arnett 1995).

The pulsar's wind is obviously the dominant force shaping the Crab's current evolution but ejecta interaction with circumstellar gas could have be affected the remnant's earlier development. The Crab's N-S expansion matches the interacting stellar winds models suggested for Eta Carinae (Frank *et al.* 1995), where the pole-to-equator density contrast exceeds 100, and a high ratio of toroidal density to ambient medium creates expansion kinematics quite similar to those of the Crab.

Fesen *et al.* (1992) proposed that the remnant's east and west synchrotron bays and the helium-rich band of filaments are the results of an interaction between the Crab's ejecta and a circumstellar disk off the progenitor. As part of their evidence, they noted a strip in the east bay nearly devoid of filaments not unlike that expected from filament deceleration along a disk. Li & Begelman (1992) proposed an alternative model were the bays were formed by interaction with the dense equatorial plane of the progenitor's slow, mass loss wind. In either scenario, such interactions could lead to an E-W expansion constriction and hence a N-S bipolar symmetry. However, high hydrogen not helium abundances would be expected in the expansion pinched zone, just the opposite of what is observed (Chevalier 1995). In addition, the nature of the bays is controversial, with Michel *et al.* (1991) interpreting them as interactions of the pulsar's magnetic field with filaments viewed along our line of sight. It is therefore uncertain whether the Crab's N-S expansion asymmetry is due to the presence of circumstellar material.

Examining 3C 58 (SN 1181), the only other young Galactic SNR with properties like those of the Crab, one does find appreciable circumstellar material present. 3C 58's optical filaments, like those of the Crab, show expansion velocities of $\sim$1000 km s^{-1}. But the remnant also contains considerable slow-moving material ($v \leqslant 200$ km s^{-1}) among the faster ejecta knots (Fesen *et al.* 1988). Preliminary findings from a spectral analysis of more than 300 of 3C 58's optical emission filaments (Fesen *et al.* 1996) show a correlation between higher filament N/H ratios and higher expansion velocities, supporting the notion of low-velocity, hydrogen-rich circumstellar matter and high-velocity, nitrogen-rich SN ejecta. A similar correlation has been found for the Crab's nitrogen distribution, where higher velocities were seen for the more N-rich filaments as expected from an acceleration of the progenitor envelope (MacAlpine *et al.* 1996). However, 3C 58's filaments show no expansion asymmetries that might indicate any interactions with circumstellar matter.

5. FILAMENT MASS AND STELLAR MASS LOSS

5.1 Mass Estimates Revisited

An additional problem with an ejecta-circumstellar interaction model is the low estimated mass for the nebula's filaments. To confine the free expansion of ejecta, a significant circumstellar mass would imply a large fractional contamination of some filaments and thus an even lower SN mass ejection. Below, we reassess previous mass estimates for the remnant's thermal gas component and show that there may be considerably more mass in the filaments than previously estimated.

Of the expected 8.6±2 $\mathcal{M}_\odot$ shed from the star (10±2 $\mathcal{M}_\odot$ in the progenitor minus a 1.4 $\mathcal{M}_\odot$ neutron star), an estimate of only 1–2 $\mathcal{M}_\odot$ was reported by MacAlpine & Uomoto (1991) in the ionized filaments. However, considerable uncertainties exist in this estimate, and it is useful to re-examine its various components, using a common Crab distance and helium abundance and adopting current atomic data. The observed global flux, $F(\mathrm{H}\beta)=(1.78\pm0.2)\times10^{-11}$ erg cm^{-2} s^{-1} (MacAlpine & Uomoto 1991), together with an assumed distance $d=(2\ \mathrm{kpc})d_2$ and extinction $A_V=1.6^m$ (Miller 1973), yields an ionized mass,

$$\mathcal{M}_{\mathrm{ion}}=\left[\frac{4\pi d^2 F(\mathrm{H}\beta)\exp(\tau_{\mathrm{H}\beta})m_{\mathrm{H}}}{\alpha_{\mathrm{eff}}(\mathrm{H}\beta)E_{\mathrm{H}\beta}n_e(1-Y)}\right]$$

$$=(1.45\ \mathcal{M}_\odot)d_2^2T_4^{0.864}n_3^{-1}\left(\frac{0.2}{1-Y}\right). \quad (7)$$

Here, we have adopted scaling factors for the filament temperature (10^4 K)T_4, the electron density (10^3 cm^{-3})n_3, and the mean helium mass fraction $Y\approx0.8$. Spectral diagnostics from [O III] and [S II] (Fesen & Kirshner 1982; Henry *et al.*1984 ; MacAlpine *et al.* 1989) give a range $T_4=1.5\pm0.3$, $n_3=1.0\pm0.5$, and $Y=0.8\pm0.1$. Thus, from a formal propagation of errors in Eq. (7), we find a "best estimate," accurate to about 40%, of $\mathcal{M}_{\mathrm{ion}}=(2.1\pm0.9)\ \mathcal{M}_\odot$. The largest sources of uncertainty in $\mathcal{M}_{\mathrm{ion}}$ are the density (n_e) and Crab distance (d_2).

The neutral filaments probed by [S II] emission (Fesen & Kirshner 1982; Henry & MacAlpine 1982) have a total dereddened flux of 4.14×10^{-10} erg cm^{-2} s^{-1}. Using current [S II] atomic data (Cai & Pradhan 1993) and an abundance S/H=1.6×10^{-5}, we find an additional neutral filament mass of

$$\mathcal{M}_{\mathrm{neut}}=(1.5\pm0.6\ \mathcal{M}_\odot)d_2^2T_4^{0.58}n_3^{-1}\left(\frac{0.2}{1-Y}\right). \quad (8)$$

Adopting $d=2$ kpc, $n_3=1$, $Y=0.8$, and $T_e=8000$ K for the [S II] neutral filaments, we find a "best value" of $\mathcal{M}_{\mathrm{neut}}=1.34\pm0.53\ \mathcal{M}_\odot$ for the neutral filaments, again accurate to about 40%.

Finally, recent detections of dense clumps containing dust and H_2 (Fesen & Blair 1990; Graham *et al.* 1990) suggest a repository for additional mass in neutral cores, over and above those traced in [S II]. A rough estimate of $1000N_3$ clumps of hydrogen column density (10^{20} cm^{-2})N_{20} and angular radius θ (in arcsec) gives a total core mass of

$$\mathcal{M}_{\mathrm{core}}=(1.2\pm0.5\mathcal{M}_\odot)d_2^2\theta^2N_{20}N_3\left(\frac{0.2}{1-Y}\right), \quad (9)$$

assigning the same 40% uncertainty as for the other masses. Since the major sources of uncertainty (n_e and d_2) are common to all three components of the nebular mass, we adopt a collective uncertainty of 40% and a total nebular mass of 4.6±1.8 $\mathcal{M}_\odot$. Note that, within a given component, these estimates assume single values for density, temperature, and helium abundance. A careful filament-by-filament He abundance survey, using appropriate diagnostics of n_e and T_e could give more accurate values.

5.2 Stellar Mass Loss

Using the above results, we can now begin to account for the amount of mass lost in the stellar winds. If we start with a 10 $\mathcal{M}_\odot$ progenitor and subtract 1.4 $\mathcal{M}_\odot$ for the neutron star and (4.6±1.8) $\mathcal{M}_\odot$ in nebular mass, the wind mass loss would total about (4±2) $\mathcal{M}_\odot$. (It could be even lower than 2 $\mathcal{M}_\odot$ if the progenitor had a mass as low as 8 $\mathcal{M}_\odot$ and the nebular mass were larger than 4.6 $\mathcal{M}_\odot$). According to recent evolutionary models (Schaller *et al.* 1992) a 10 $\mathcal{M}_\odot$ star should lose 0.4–0.8 $\mathcal{M}_\odot$ in stellar winds over its lifetime, prior to the episode of bipolar mass loss discussed above. The blue supergiant mass loss would then be contained in a wind-driven bubble 20–30 pc from the Crab, while the slow red giant wind should be confined to radii ~10 pc [see Eq. (3)].

Finally, we examine whether our mass estimate (4.6±1.8 $\mathcal{M}_\odot$) for the nebula, violates abundance expectations from stellar models. If the helium mass fraction $Y=0.8$, the nebula contains 3.7±1.4 $\mathcal{M}_\odot$ of helium. Recent models of massive-star supernova nucleosynthesis (Woosley & Weaver 1995) yield the following masses of ejected helium and oxygen for progenitors of 11–13 $\mathcal{M}_\odot$:

$$\mathcal{M}=11\mathcal{M}_\odot:\mathcal{M}_{\mathrm{He}}=3.73\mathcal{M}_\odot,\quad \mathcal{M}_{\mathrm{O}}=0.14\ \mathcal{M}_\odot, \quad (10)$$

$$\mathcal{M}=12\mathcal{M}_\odot:\mathcal{M}_{\mathrm{He}}=4.11\mathcal{M}_\odot,\quad \mathcal{M}_{\mathrm{O}}=0.22\ \mathcal{M}_\odot, \quad (11)$$

$$\mathcal{M}=13\mathcal{M}_\odot:\mathcal{M}_{\mathrm{He}}=4.51\mathcal{M}_\odot,\quad \mathcal{M}_{\mathrm{O}}=0.27\ \mathcal{M}_\odot. \quad (12)$$

Therefore, our standard estimate (nebular mass of 4.6 $\mathcal{M}_\odot$ and $\mathcal{M}_{\mathrm{He}}=3.7\ \mathcal{M}_\odot$ for $Y=0.8$) suggests a Crab progenitor mass range of 10–11 $\mathcal{M}_\odot$, consistent with other estimates. Considerable uncertainties in the nebular mass still exist, particularly in the helium abundance, Y, which varies among filaments from 0.5 to 0.9. However, we believe that our estimates are more careful than the earlier estimates of the ionized filament mass: [1.5 $\mathcal{M}_\odot$ by Henry & MacAlpine (1982); (4.5–7.5)$\mathcal{M}_\odot$ by MacAlpine *et al.* (1989); and (1–2) $\mathcal{M}_\odot$ by MacAlpine & Uomoto (1991)].

Detailed modeling of the ionized filaments and the dense and dusty clumps might account for most of the mass discrepancy. Indeed, the bipolar outflow suggested by the N-S filament expansion asymmetry might be the signature of the bulk of the red supergiant mass loss. In that case, observers will have to work much harder to detect the "Crab shell"

arising from the earlier mass loss that occurred during the red giant stage.

6. CONCLUSIONS

We have presented new optical spectral data probing the presence of emission around the Crab Nebula. We also have investigated asymmetries in the N-S filament expansion and have re-analyzed the remnant's possible total mass. Our major conclusions are the following:

(1) Long-slit spectra taken at two peripheral regions of the Crab Nebula, the NW limb and the northern jet, show no evidence for an optical halo in Hα or any other line between 4600 and 7000 Å. No Hα emission was detected out to a radius of 3.4′ down to 1.5×10^{-7} erg cm^{-2} s^{-1} sr^{-1}. This translates to an Hα emission measure limit of 4.2 cm^{-6} pc^{-1} (3σ) assuming $A_V=1.6^{\rm m}$ and $T_e=7000$ K, below the flux level reported by Murdin & Clark (1981) for an Hα halo around the remnant. This negative result raises doubts as to the reality of a halo surrounding the Crab as bright as claimed by Murdin & Clark (1981).

(2) We have investigated the faint Hβ emission surrounding the Crab reported by Murdin (1994) and find that weak Hβ emission is indeed present in the local vicinity of the remnant. However, contrary to Murdin's conclusion, this emission appears to be diffuse Galactic emission and not associated with the remnant since it disappears after sky subtraction using a sky spectrum taken outside the reported halo.

(3) Reviewing earlier searches for a high-speed shock front or extended halo around the remnant, we conclude that there is as yet no observational support for a high- or low-velocity envelope around the Crab Nebula as has been proposed on theoretical grounds (Chevalier 1977, 1985).

(4) Long-slit scans of both the whole remnant and smaller sections confirm a smooth, remnant-wide N-S expansion asymmetry. This structure has a ~500 km s^{-1} central velocity constriction due to a chain of east-west filaments as found by MacAlpine *et al.* (1989) and Lawrence *et al.* (1995) but questioned by Hester *et al.* (1995, 1996). The N-S velocity pinching coincides with the remnant's brightest [O III] and highest helium-rich filaments. It is currently unclear whether such a N-S expansion asymmetry is due to pre-supernova circumstellar mass loss that partially confined and mixed with the emerging SN ejecta, or simply an asymmetry in the SN ejecta outflow.

(5) A reanalysis of the remnant's total nebular mass suggests that the filamentary nebula may contain $(4.6\pm1.8)\,\mathcal{M}_\odot$ in ionized and neutral filaments and dense clumps, about twice that of prior estimates. This additional mass may be in neutral filament cores assuming an average helium mass fraction $Y\approx0.8$. This higher filament mass estimate removes much of the remnant's low-mass discrepancy.

We thank the staff of NOAO for help with the Burrell Schmidt telescope and R. Finn and the MDM Observatory staff for observing assistance and instrument setup. We are also grateful to the referee for several helpful comments. This work was supported by a Walter Burke Grant at Dartmouth and by the Astrophysical Theory Program (NASA Grant No. NAGW-766) at the University of Colorado.

REFERENCES

Bietenholtz, M. F., *et al.* 1991, ApJ, 373, L59
Bjorkman, J. E., & Cassinelli, J. P. 1993, ApJ, 409, 429
Blair, W. P., *et al.* 1992, ApJ, 399, 611
Blondin, J. M., & Lundqvist, P. 1993, ApJ, 405, 337
Bond, H. E., & Livio, M. 1990, ApJ, 355, 568
Cai, W., & Pradhan, A. K. 1993, ApJS, 88, 329
Cardelli, J., Clayton, G., & Mathis, J. 1989, ApJ, 345, 245
Chevalier, R. A. 1977, in Supernovae, edited by D. N. Schramm (Reidel, Dordrecht), p. 53
Chevalier, R. A. 1985, in The Crab Nebula and Related Supernova Remnants, edited by M. C. Kafatos and R. B. C. Henry (Cambridge University Press, Cambridge), p. 63
Chevalier, R. A. 1995, in Supernovae and Supernova Remnants, IAU Colloquium 145, edited by R. McCray and Z. Wang (Cambridge University Press, Cambridge), p. 399
Chevalier, R. A., & Fransson, C. 1992, ApJ, 395, 540
Clark, D. H., & Stephenson, F. R. 1977, The Historical Supernovae (Pergamon, Oxford)
Clark, D. H., Murdin, P., Wood, R., Gilmozzi, R., Danziger, J., & Furr, A. W. 1983, MNRAS, 204, 415
Davidson, K. 1987, AJ, 94, 964
Davidson, K., & Fesen, R. A. 1985, ARA&A, 23, 119
Fesen, R. A., & Gull, T. R. 1986, ApJ, 306, 259
Fesen, R. A., & Blair, W. P. 1990, ApJ, 351, L45
Fesen, R. A., Hurford, A. P., & Soto, A. 1996, in preparation
Fesen, R. A., & Ketelsen, D. A., 1985, in The Crab Nebula and Related Supernova Remnants, edited by M. C. Kafatos and R. B. C. Henry (Cambridge University Press, Cambridge), p. 89
Fesen, R. A., & Kirshner, R. 1982, ApJ, 258, 1
Fesen, R. A., Kirshner, R. P., & Becker, R. H. 1988, in Supernova Remnants and the Interstellar Medium, IAU Colloquium 101, edited by R. S. Roger and T. L. Landecker (Cambridge University Press, Cambridge), p. 55
Fesen, R. A., Martin, C. L., & Shull, J. M. 1992, ApJ, 399, 599
Fesen, R. A., & Staker, B. 1993, MNRAS, 263, 69
Frail, D. A., Kassim, N. E., Cornwell, T. J., & Goss, W. M. 1995, ApJ, 454, L129
Frank, A., Balick, B., & Davidson, K. 1995, ApJ, 441, L77
Graham, J. R., Wright, G. S., & Longmore, A. J. 1990, ApJ, 352, 172
Gull, T. R., & Fesen, R. A. 1982, ApJ, 260, L75
Henry, R. B. C., & MacAlpine, G. M. 1982, ApJ, 258, 11
Henry, R. B. C., MacAlpine, G. M., & Kirshner, R. P. 1984, ApJ, 278, 619
Hester, J. J., *et al.* 1995, ApJ, 448, 240
Hester, J. J., *et al.* 1996, ApJ, 456, 225
Humphreys, R. M., & Davidson, K. 1994, PASP, 106, 1025
Lawrence, S. S., MacAlpine, G. M., Uomoto, A., Woodgate, B. E., Brown, L. W., Oliverson, R. J., Lowenthal, J. D., & Liu, C. 1995, AJ, 109, 2635
Li, Z.-Y., & Begelman, M. C. 1992, ApJ, 400, 186
Lundqvist, P., Fransson, C., & Chevalier, R. 1986, A&A, 162, L6
Luo, D., & McCray, R. 1991, ApJ, 379, 659
MacAlpine, G. M., McGaugh, S. S., Mazzarella, J. M., & Uomoto, A. 1989, ApJ, 342, 364
MacAlpine, G. M., & Uomoto, A. 1991, AJ, 102, 218
MacAlpine, G. M., Lawrence, S. S., Sears, R. L., Sosin, M. S., & Henry, R. B. C. 1996, ApJ, 463, 650
Mauche, C. W., & Gorenstein, P. 1989, ApJ, 336, 843
Marcalde, J. M., *et al.* 1995, Nature 373, 44
Marcelin, M., Boulesteix, J., Véron-Cetty, M. P., Woltjer, L., & D'Odorico, S. 1990, A&A, 228, 471

Martin, C. L., & Arnett, D. 1995, ApJ, 447, 378
Michel, F. C., Scowen, P. A., Dufour, R. J., & Hester, J. J. 1991, ApJ, 368, 463
Miller, J. S. 1973, ApJ, 180, L83
Murdin, P. 1994, MNRAS, 269, 89
Murdin, P., & Clark, D. H. 1981, Nat, 294, 543
Nomoto, K. 1985, in The Crab Nebula and Related Supernova Remnants, edited by M. C. Kafatos and R. B. C. Henry (Cambridge University Press, Cambridge), p. 97
Nomoto, K. 1987, in The Origin and Evolution of Neutron Stars, IAU Symposium 125, edited by D. J. Helfand and J.-H. Huang (Reidel, Dordrecht), p. 281
Nomoto, K., Sparks, W. M., Fesen, R. A., Gull, T. R., Miyaji, S., & Sugimoto, D. 1982, Nat, 299, 803
Oke, J. B. 1974, ApJS, 27, 21
Osterbrock, D. E. 1989, Astrophysics of Gaseous Nebulae and Active Galactic Nuclei (University Science Books, Mill Valley, CA)
Podsiadlowski, Ph., Hsu, J. J. L., Joss, P. C., & Ross, R. R. 1993, Nature, 363, 509
Predehl, P., & Schmidt, J. H. M. M. 1995, A&A, 293, 887
Pskovskii, Y. P. 1978, Sov. Astron. AJ, 22, 420
Reynolds, R. J. 1988, ApJ, 333, 341
Romani, R. W., Reach, W. T., Koo, B.-C., & Heiles, C. 1990, ApJ, 349, L51
Schaller, G., Schaerer, D., Meynet, G., & Maeder, A. 1992, A&AS, 96, 269
Shull, Jr., P., Carsenty, U., Sarcander, M., & Neckel, T. 1984, ApJ, 285, L75
Stone, R. P. S. 1977, ApJ, 218, 767
Trimble, V. 1973, PASP, 85, 579
Trushkin, S. A. 1986, Pis'ma Astron. Zhurnal, 12, 198
Uomoto, A., & MacAlpine, G. M. 1987, AJ, 93, 1511
Vacca, W. D., Garmany, C. D., & Shull, J. M. 1996, ApJ, 460, 914
Véron-Cetty, M. P., Véron, P., & Woltjer, L. 1985, A&A, 151, 101
Velusamy, T. 1984, Nat, 308, 251
Velusamy, T. 1985, MNRAS, 212, 359
Velusamy, T., Roshi, D., & Venugopal, V. R. 1992, MNRAS, 255, 210
Wallace, B. J., Landecker, T. J., & Taylor, A. R. 1994, A&A, 286, 565
Wheeler, J. C. 1978, ApJ, 225, 212
Wilson, A. S., & Weiler, K. W. 1982, Nature, 300, 155
Woosley, S., & Weaver, T. A. 1995, ApJS, 101, 181
Wyckoff, S., & Murray, C. A. 1977, MNRAS, 180, 717

PLATE 15

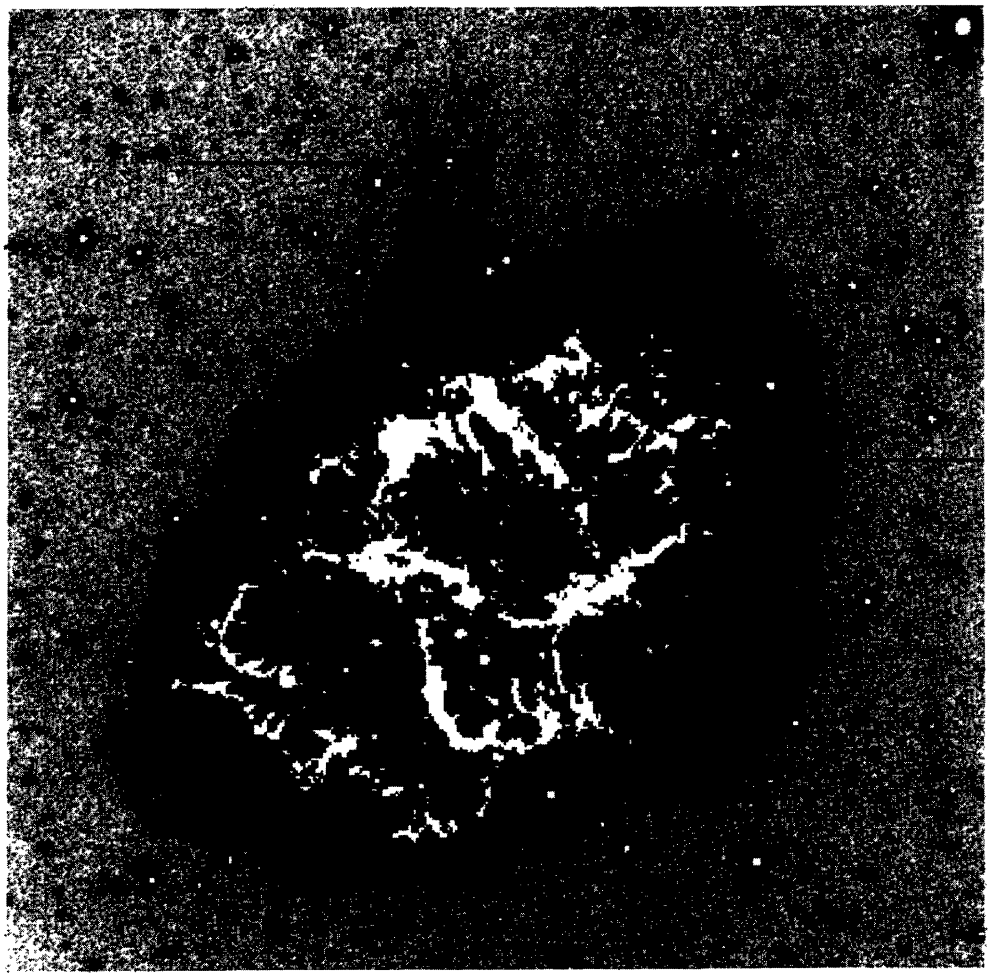

FIG. 1. Deep [S II] image of the Crab Nebula showing slit positions along the NW limb (right) and northern jet (top). The western end of the NW slit extends off the edge of the image. The remnant's bright inner filaments are shown as white features. North is to the top, east to the left.

Fesen *et al.* (see page 355)